Structure of the $c(2\times2)$-Br/Pt(110) surface

V. Blum, L. Hammer, and K. Heinz
Lehrstuhl für Festkörperphysik, Institut für Angewandte Physik, Staudtstrasse 7-A3, D-91058 Erlangen, Germany

C. Franchini* and J. Redinger
Center for Computational Materials Science, Vienna University of Technology, Getreidemarkt 9, A-1060 Vienna, Austria

K. Swamy, C. Deisl, and E. Bertel
Institut für Physikalische Chemie, Unversität Innsbruck, Innrain 52a, A-6020 Innsbruck, Austria
(Received 14 September 2001; published 4 April 2002)

We present a detailed investigation of the $c(2\times2)$-Br/Pt(110) adlayer structure supplemented by the analysis of the (1×2) missing-row (MR) structure of the clean Pt(110) surface. Quantitative low energy electron diffraction analyses and first-principles calculations are in impressive agreement in both cases. The clean surface reconstruction is determined with unprecedented accuracy. For the adsorbate, the analysis retrieves a simple Br-adlayer structure with the Br atoms residing in every second short bridge position on the close-packed Pt rows with the MR reconstruction lifted. The Br-Pt bond length $L=2.47$ Å is almost equal to the sum of the atomic radii. The substrate below the adsorbate exhibits a contraction of the first layer spacing which amounts to half of that calculated for an unreconstructed clean surface.

DOI: 10.1103/PhysRevB.65.165408 PACS number(s): 68.43.Fg, 61.14.Hg, 68.43.Bc, 68.37.Ef

I. INTRODUCTION

Halogens interact strongly with all metal surfaces. For this reason they play an important role in many technically important processes. For instance, halogens are strongly corrosive. By the same token they may be used for surface etching.[1] As strong adsorbates, they efficiently poison several catalytic reactions, but are also used as promoters in particular cases.[2] Finally, they are interesting candidates to study within the context of self-structuring. Due to their high adsorption energy one may anticipate halogen-induced reconstruction, but also major changes in the surface stress and consequently the *mesoscopic* surface morphology.[3] In addition, the well-known tendency of halogen-bridged transition-metal linear-chain compounds to form competing ground states [such as charge density waves (CDW's) or spin density waves[4]] renders halogen adsorption on anisotropic surfaces an interesting candidate to study these low-dimensional phenomena on surfaces.[5]

There are, however, only few studies dealing with the quantitative determination of the geometric structure of halogens on metals. In most previous studies, the structure was deduced from qualitative low energy electron diffraction (LEED)[6–11] or scanning tunneling microscopy (STM).[3,12–16] Adsorption site analysis was carried out mainly by surface extended x-ray-absorption fine structure (SEXAFS),[17–23] whereas quantitative structure determinations by LEED (Refs. 24–26) or first-principles calculations[27,28] are sparse.

In all quantitative halogen adsorption studies a simple adsorption layer (simple overlayer model in Ref. 18) is favored over substitutional adsorption (mixed-layer model in Ref. 18) for halogen coverages up to 0.5 monolayers (ML). For higher coverages, however, the formation of a metal-halogen corrosion layer is observed for different low-index Ag surfaces.[29]

As an example, Cl/Cu(111) represents a well-studied system, investigated by, e.g., SEXAFS,[19] normal incident x-ray standing wave field absorption (NIXSW),[30] and DFT calculations.[27] Cl is found to adsorb in the fcc hollow site forming a simple overlayer. In the case of (100) surfaces, simple adsorption in the fourfold hollow site is favored, e.g., by a LEED structure analysis [Cl/Ag(100),[24,31] Cl/Cu(100) (Refs. 25,26)] and SEXAFS studies [I/Cu(100),[17] Cl/Cu(100) (Refs. 18,23)]. With regard to halogen adsorption on the more open (110) surfaces of fcc metals, there are no quantitative studies of the adsorption structure. In most investigations simple adsorption was assumed.[3,6–9,12,15] A cluster calculation for I/Ag(110) (Ref. 28) favors the short bridge position as adsorption site.

In a previous paper[16] some of the authors presented a study of Br/Pt(110) mainly based on STM and qualitative LEED measurements. For a Br coverage of $\Theta=0.5$ ML a $c(2\times2)$ structure was found. It was interpreted as a substitutional structure due to reasons discussed in Ref. 16 and in Sec. IV of this paper. However, a quantitative LEED investigation, which is based on intensity measurements carried out under identical preparation conditions (in the same lab), as well as a DFT analysis, both discussed in the present paper, clearly prove a simple adlayer structure instead of a substitutional adsorption site. The close quantitative correspondence between the structural parameters derived from both independent methods leaves no room for alternative models. The adsorption site found in this study is also favored by new atom-resolved low-coverage STM images.[32] These new results imply that our previous conclusions for general substitutional adsorption in the case of halogens on metal fcc(110) surfaces have to be revised. We emphasise, however, that the new adsorption model does not change our conclusions with regard to the one dimensionality of the $c(2\times2)$-Br/Pt(110) structure.

The paper is organised as follows. In Sec. II we present experimental and computational details of the investigations.

In Sec. III the missing-row (MR) reconstruction of clean Pt(110) is reanalyzed both by means of LEED and DFT. The metastable Pt(110)-(1×1) structure was analyzed as well by means of DFT. The structural results for the $c(2\times2)$-Br/Pt(110) surface derived from LEED and DFT are presented and discussed in detail in Sec. IV. This section concludes with a reinterpretation of former experimental results from Ref. 16 in the light of the newly determined bromine adsorption structure. The paper closes with a summary.

II. EXPERIMENTAL AND COMPUTATIONAL DETAILS

The experiments were performed in a UHV chamber (base pressure $<8\times10^{-11}$ mbar) equipped with a commercial STM (Ref. 33) and control electronics,[34] a four-grid LEED system,[35] and the usual facilities for sample preparation and characterization. The preparation of the Pt(110) crystal according to the standard procedure[36] resulted in a clean surface showing the well known 1×2 superstructure originating from the missing-row reconstruction. The LEED spots are rather intense, but somewhat elongated in the [001] direction, as was also reported in earlier LEED studies (e.g., Ref. 37). This broadening is due to small terrace widths of only about 15 Å on average for this direction due to the mesoscopic ''corrugated-iron'' structure found for this surface.[36,38] Bromine molecules were dosed at $T\approx130$ K by means of a solid-state electrolysis cell. Annealing of the sample at 780 K leads to partial bromine desorption leaving 0.5 ML of dissociated Br on the surface (for details of the preparation see Ref. 16). The resulting STM images [see Fig. 1(a)] show a well-ordered $c(2\times2)$ structure with only occasional $p(2\times1)$ regions near defects and steps. Consistently, the corresponding LEED pattern is also of $c(2\times2)$ symmetry with clear superstructure spots of moderate intensity compared to that of the substrate spots [Fig. 1(c)]. Additionally, however, there are faint streaks in [001] direction through the superstructure spots as well as some diffuse intensities at $[(2m-1)/2,n]$ positions [corresponding to a $p(2\times1)$ periodicity] indicative of residual disorder. This can be understood in terms of antiphase domains in [001] direction and/or small coexisting $p(2\times1)$ patches at the surface. Such a coexistence of $c(2\times2)$ and $p(2\times1)$ phases was found in STM below the optimum annealing temperature needed for the well-ordered $c(2\times2)$ structure and at defects and steps.[16] Entire LEED patterns taken at normal primary beam incidence and with the sample at about 130 K were recorded in steps of 0.5 eV in the energy range 40–500 eV by means of a 12-bit digital CCD camera[39] (images were sampled 8 times). They were stored on a computer for offline evaluation of sufficiently intense beams. The beam intensities resulted by pixelwise summation within a certain frame around a spot whereby the background level determined at the frame's edges was subtracted. Spectra of beams symmetrically equivalent at normal incidence were eventually averaged and slightly smoothed when necessary, followed by normalization to the primary beam intensity. For the 1×2 missing-row structure of the clean surface this procedure resulted in a data set of 16 integer and 11 fractional order beams with integrated energy widths of 3761 and 2587 eV, respectively, yielding a total data base width of as much as $\Delta E=6348$ eV. For the $c(2\times2)$-Br adsorbate phase ten integer order (3297 eV) and four fractional order (1289 eV) beams were taken with a total energy width of $\Delta E=4586$ eV.

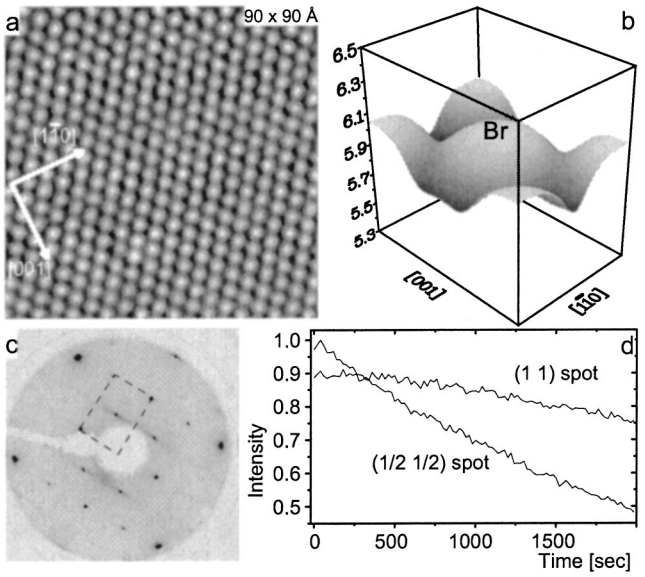

FIG. 1. (a) STM image of the $c(2\times2)$-Br/Pt(110) surface ($I_t=0.87$ nA, $V_t=820$ mV). The contrast is 0.25 Å. (b) Calculated STM image from FLEUR-GGA-9L results: A constant current STM image for an energy range equivalent to (a) shows Br appearing as a protrusion with a corrugation amplitude of 0.25 Å at a tip Pt-surface distance of ~6 Å. Vertical distances (in Å) are given with respect to the top Pt layer. (c) Corresponding LEED pattern ($U=147$ eV). (d) (1,1) and (1/2,1/2) spot intensity as a function of time at $U=147$ eV (see Sec. IV C).

LEED intensity calculations were performed using the TENSERLEED program package.[40] This applies the Tensor LEED perturbation scheme,[41–43] extended to allow not only for the variation of the surface geometry but also for that of vibrational parameters.[44,45] For a certain reference structure a full dynamical calculation is carried out and intensity changes due to (small) deviations from this reference are calculated by perturbation. The structural search is made by a frustrated simulated annealing procedure[46] and guided by the Pendry *R*-factor R_P (Ref. 47) for the quantitative comparison of experimental and calculated spectra. Electron attenuation was described by an imaginary part of the optical potential V_{0i}. It was adjusted for the clean surface resulting in a constant value of $V_{0i}=6$ eV and the same value was used for the Br adsorbate phase. The real part of the inner potential V_{0r} was allowed to be energy dependent according to the variation of the exchange-correlation potential with energy. Following the literature[48] the expression $V_{0r}=V_{00}+\max(-10.64\ \text{eV}, 0.63\ \text{eV}-85.10\ \text{eV}/\sqrt{E/\text{eV}+17.02})$ was used with only the constant part fitted to the spectra which resulted in $V_{00}=-0.5$ eV for the clean and $V_{00}=0$ eV for the bromine covered surface. As much as 14 fully relativistically calculated and spin averaged phase shifts were used, sufficient to describe the atomic scattering up to the maximum energy of 500 eV. They were corrected for isotropic

thermal vibrations with fixed amplitude $v_b = 0.07$ Å for bulk atoms and of variable (i.e., to be fitted) amplitudes for atoms in layers in the vicinity of the surface. For the bulk of the platinum sample the lattice parameter 3.923 Å was used corresponding to a surface parallel in-plane value of 2.774 Å.

Attention had to be paid not to leave the validity range of tensor LEED during the structural fit procedure. Therefore, new reference calculations were carried out whenever new points reached in the parameter space were too distant from the former reference until convergence was achieved. Statistical error limits for the varied parameters were estimated through the variance of the Pendry R factor[47] $\mathrm{var}(R_P) = R_P\sqrt{8V_{0i}/\Delta E}$ with R_P the minimum R factor. All structures with R factors below $[R_P + \mathrm{var}(R_P)]$ are supposed to be within the limits of error. This procedure takes the different sensitivities of the R factor with respect to the different parameters into account. In principle one should also consider correlations between different parameters, but this involves extremely time consuming calculations and so the influence of such correlations was neglected in the present work. This is actually the standard in LEED structure determination. Accordingly, the error limits for a certain parameter were determined by the R factor's crossing of the variance level with variation of the parameter under consideration but all other parameters kept fixed at their best-fit values. We point out that this neglect of correlations generally underestimates the error limits. For simple structures, for which their consideration is still possible, we found that the true error is about twice that resulting by the neglect of correlations,[49] so this might give a rough idea for the true errors. We also point out that atomic positions not varied and so possibly not correctly taken into account lead to an increased R factor and, as a consequence, to an increased variance level.

First principles density functional theory (DFT) calculations were performed using both, the all-electron full-potential linearized augmented plane wave (FLAPW) method,[50] as implemented in the package FLEUR,[51] and the Vienna *ab initio* simulation package (VASP) (Ref. 52) with the projector augmented wave[53] method as implemented by Kresse and Joubert.[54]

Throughout this work two DFT potential approximations have been used: the generalized gradient approximation (GGA) according to Perdew and Wang (PW91) (Ref. 55) and the local density approximation (LDA) in the Perdew-Zunger (Ceperly-Alder) parametrization scheme.[56,57] The surface was modeled using a slab of up to 15 layers thickness, repeated along the surface normal for VASP, and a single slab with vacuum on both sides for FLEUR. In VASP the repeated slabs are separated by a vacuum layer of at least 8 Å.

In FLEUR calculations a symmetric (with respect to the middle layer) nine layer slab was used, allowing four layers to relax. Well converged results were obtained for plane wave cutoff $k_{\max} = 3.7$ a.u. Inside the muffin-tin spheres, the angular momentum expansion was taken up to $l_{\max} = 8$, both for the full-potential and charge-density representation. The core electrons, including the $5p$ states, were treated fully relativistically and the valence electrons derived from the atomic $5d$, $6s$, and $6p$ orbitals are treated semirelativistically, i.e., dropping only the spin-orbit term in the Hamiltonian. The k-mesh consisted of 16 special points in the irreducible wedge of the strictly two-dimensional Brillouin-zone chosen according to Cunningham.[58]

For the VASP calculations an energy cutoff of about 230 eV and a $6\times6\times1$ Monkhorst-Pack type k-point mesh turned out to generate results sufficiently accurate for the present purposes. Due to its high efficiency, VASP allows one to treat thicker slabs within a reasonable computing time. For example, the accuracy of our calculations as a function of slab thickness was checked by performing VASP calculations for a 15 layers slab where 4 layers on one side had been frozen to bulk geometry. Allowing the remaining 11 layers to relax, errors in the final calculated geometry due to finite slab effects for all the different structure models investigated, can be tracked easily. Finally, for both methods, the geometry was optimized until all forces were smaller than 0.01 eV/Å.

III. REANALYSIS OF THE CLEAN RECONSTRUCTED PT(110) SURFACE

Though the low temperature equilibrium structure of the clean Pt(110) surface is known since long to be of the missing-row type, there is a remarkable scatter in the structural parameters determined both in experimental[37,59–63] and theoretical[64–67] studies. In experiment one might argue that these differences simply stem from varying preparation conditions. Yet, they may also be caused by computer limitations holding at the time these studies were performed. Therefore, it appeared reasonable to reanalyse the clean surface on the grounds of today's standards in structure determination by LEED and DFT. Simultaneously, a close correspondence between the results of the two methods would give some confidence for their successful application to the yet unknown bromine adsorbate system.

A. LEED results for the 1×2 missing-row structure

There is no doubt concerning the validity of the missing-row model for Pt(110)-(1×2). Hence only parameters describing this model were varied in the course of the structure determination. Intensities were calculated up to energies of 500 eV in order to use the whole experimental data base width of $\Delta E = 6348$ eV. This unusually large value leads to a rather low value of the variance of the R factor and consequently promises a correspondingly high accuracy of the analysis. Fit parameters were the outermost five layer spacings $d_{i,i+1}$ $(i=1-5)$, vertical bucklings b_3 and b_5 within the third and fifth layer, respectively, lateral pairing amplitudes p_2 and p_4 between neighboring atoms in [001] direction within the second and fourth layer, respectively, as well as the (isotropic) vibrational amplitudes v_i for the outermost three layers $(i=1-3)$. The variational grid width for fit parameters was usually set to 0.01 Å. All other parameters were kept fixed at their bulk values. In order to allow for an unbiased approach to the best-fit geometry the search was started with bulklike interatomic distances. As a consequence, it took three reference calculations to approach the best-fit structure and to stay always within the validity range

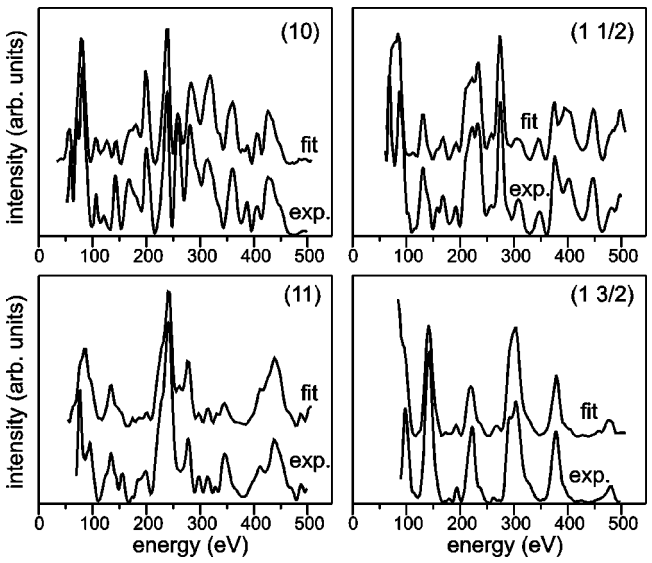

FIG. 2. Comparison of experimental and calculated best-fit LEED-I(E) spectra for the missing-row reconstruction of clean Pt(110).

of tensor LEED. The quality of agreement between experimental and calculated best-fit spectra is displayed in Fig. 2 for a selection of beams. The minimum R factor amounts to $R_P=0.22(5)$, whereby both subsets of integer and fractional order beams exhibit very similar fit qualities $[R_P^{\mathrm{int}}=0.21(6), R_P^{\mathrm{frac}}=0.23(6)]$. Additionally, the ratio r between energy averaged intensities of fractional and integer order beams $r=\langle I\rangle_{\mathrm{frac}}/\langle I\rangle_{\mathrm{int}}$, fits very well, too ($r_{\mathrm{exp}}=0.46, r_{\mathrm{calc}}=0.45$).

The reader might argue that the R-factor fit level is only modest in view of values in the range 0.1–0.2 (or even lower) reported repeatedly in the literature (including contributions of our own group). We point out, however, that the value achieved in the present work is still among the best ever reached for a fcc(110) surface (see Ref. 68) and a significant improvement when compared to earlier LEED structure determinations of Pt(110)-(1×2) ($R_P=0.36$ in Ref. 37; Ref. 59 uses a noncomparable multi-R-factor average). The reason for the generally higher R factors for this class of surfaces seems to come from the spectra's unusual structural richness (extrema, shoulders, etc.) to which the Pendry R factor is extremely sensitive as it is based on the logarithmic derivatives rather than the mere intensity level. Another reason might be the high step density connected with the mesoscopic corrugated-iron structure of the Pt(110)-(1×2) surface which has been discussed in Refs. 36,38.

All structural best fit parameters together with their error margins are summarized in Table I (the comparison to other results will be discussed in Sec. IV C). Our fit reproduces the well-known features of the missing-row reconstruction, which is displayed in Fig. 3. Atoms of the first half occupied layer are strongly relaxed inward by $\Delta d_{12}=-0.24$ Å pushing those directly below further into the bulk. This, in turn, leads to an extremely buckled third and slightly buckled fifth layer. Additionally, by this process neighboring atoms in the

TABLE I. Compilation of experimental and theoretical results for the 1×2 missing-row structure of clean Pt(110). $\Delta d_{i,i+1}$ denotes the changes in the (average) inter-layer spacing with respect to the ideal bulk interlayer spacing d_0, while p_i and b_i denote the lateral pairing and buckling in layer i, respectively (all values in Å). Error limits for the parameters derived by the present LEED analysis (neglecting parameter correlations) are ±0.02 Å for $\Delta d_{i,i+1}$, ±0.05 Å for b_i and ±0.07 Å for p_i. (L: number of layers considered in calculations.)

Method Experiment	Ref.	Δd_{12}	Δd_{23}	Δd_{34}	Δd_{45}	Δd_{56}	b_3	b_5	p_2	p_4	p_6	d_0
LEED	present	−0.24	−0.01	0.02	0.02	−0.01	0.26	0.03	0.07	0.13		1.385
LEED	37	−0.28	−0.01	0.02	0.01	0.01	0.17	0.03	0.08	0.10		1.385
LEED	59	−0.26	−0.18	−0.12	−0.01		0.32		0.13	0.24		1.385
MEIS	60	−0.22	0.06				0.10					1.385
XRD	61	−0.27	−0.11						0.10	0.08		1.385
RHEED	62	−0.37	0.07				0.18		0.08			1.385
RHEED	63	−0.34	−0.01				0.12		0.09			1.385
Theory												
VASP-LDA-15L	present	−0.26	−0.01	0.02	0.01	0.00	0.32	0.03	0.04	0.12	0.05	1.382
VASP-GGA-15L	present	−0.27	0.00	0.03	0.01	0.01	0.33	0.04	0.06	0.13	0.03	1.408
VASP-GGA-9L	present	−0.25	−0.02	0.03	0.01		0.37		0.01	0.18		1.408
FLEUR-GGA-9L	present	−0.23	0.00	0.02	0.00		0.37		0.01	0.19		1.405
FLAPW	67	−0.24	0.01				0.25		0.04	0.11		1.385
Tight binding	64	−0.11	0.02	−0.03	0.00				0.04			1.385
Emb. atom	65	−0.25	−0.07	0.01			0.11		0.05	0.08		1.385
Emb. atom	70	−0.26	−0.06				0.23		0.09			1.385
LO-MD	66	−0.33	−0.08	0.03			0.24		0.05	0.05		1.415

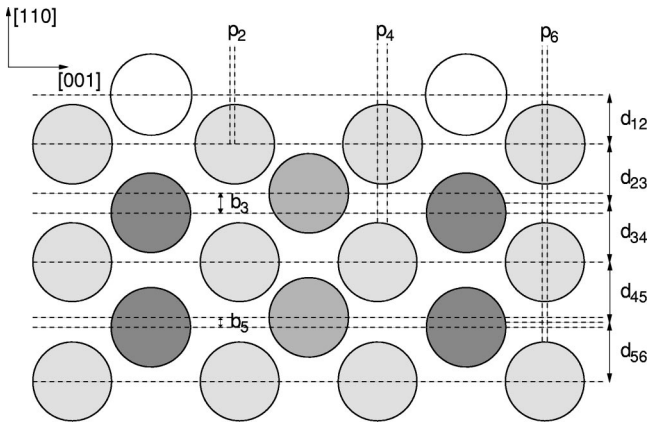

FIG. 3. Geometry of the Pt(110)$-(1\times2)$ MR surface.

second and fourth layer are squeezed a bit apart. This results in a lateral pairing of atoms within those layers. Though there are remarkable distortions within several layers, the average interlayer distances below the second layer hardly deviate from the bulk value. The vibrational amplitudes of atoms in the first three layers are as expected, i.e., the highest value applies to the outermost layer ($v_1=0.11$ Å), the vibrations in the following layers ($v_2=0.10$ Å; $v_3=0.08$ Å) approach the bulk value ($v_b=0.07$ Å). In agreement with common experience, however, the fit is not very sensitive to these parameters as reflected by error limits of ±0.04 Å for all three amplitudes.

B. DFT results for the unreconstructed 1×1 and the 1×2 missing-row structure

The results of our structural optimization for the MR surface are given in the ''theory'' part of Table I. The theoretical interlayer spacings d_0 used were obtained from bulk calculations performed by the respective methods. It is satisfying to realize that the GGA-d_0 values obtained by VASP and FLEUR are almost identical, 1.408 and 1.405 Å, respectively, with only a slight overestimation of the lattice parameter (experimental value 1.385 Å). On the contrary, the VASP LDA-d_0 value 1.382 Å is in very good agreement with the experimental value. For all other calculated spacings and pairings our two theoretical approaches, FLEUR and VASP, give also very similar results and are in excellent agreement with the experimental results of the present work, as will be discussed in more detail in the next section. Obviously, due to the openness of the mr surface, the number of layers (thickness of the slab) considered in the calculations plays a non-negligible role. In fact, for the vertical buckling b_3 one notices a considerable difference ($\approx13\%$) betweeen the results from the 9- and 15-layer calculation. Furthermore, the pairings in the second and fourth layer, albeit small, also experience considerable modifications. So, in the 9-layer calculation p_2 almost vanishes and p_4 is by about 50% larger than the 15-layer value, the latter agreeing with our experimental result. We interpret these findings as follows: In the thicker slab, which models the actual semi-infinite system best, more atoms can relax. Consequently, since the energy gained is distributed over a larger set of interlayer and intralayer spacings, relaxations take place more gradually. Thus, the rearrangement of atoms is found to extend down to the sixth layer. In a thinner slab, as, e.g., for the present symmetric 9-layer slab, relaxations can only affect four layers, giving rise to larger local changes. Clearly, both slabs give similar trends, but for the 9-layer slab the pairing is restricted to the top region only, and therefore is larger.

TABLE II. Comparison of calculated changes in inter-layer spacings of the metastable unreconstructed Pt(110)$-(1\times1)$ surface. $\Delta d_{i,i+1}$ denote the changes in the inter-layer spacing with respect to the ideal bulk interlayer spacing d_0 in Å. (L: number of layers considered in present calculations.)

Method	Ref.	Δd_{12}	Δd_{23}	Δd_{34}	Δd_{45}	Δd_{56}	d_0
FLEUR-GGA-9L	present	−0.22	0.14	−0.05			1.405
VASP-GGA-9L	present	−0.23	0.15	−0.05			1.408
VASP-LDA-15L	present	−0.22	0.11	−0.03	0.00	0.00	1.382
VASP-GGA-15L	present	−0.23	0.12	−0.04	−0.01	0.00	1.408
LCAO	77	−0.16	0.07	−0.02			1.377
Tight binding	64	−0.06	0.01	0.00			1.415
Emb. atom	86	−0.24	0.04				1.385

The results for the unreconstructed surface are listed in Table II. The 9-layer slab results by VASP and FLEUR, which are compared in the first two lines of the table, are in excellent agreement with each other. For an even more systematic comparison of the methods, FLEUR was also run in the repeated slab mode for the present surface, which further supports the equivalence of both packages with respect to accuracy. Both methods predict an inward relaxation of the topmost surface layer and of the third layer, only partially compensated by an outward relaxation of the subsurface layer. Going to thicker slabs, investigated only by VASP, mainly subsurface relaxations are reduced, e.g., Δd_{23} by 0.03 Å. Obviously, there are no significant interlayer relaxations deeper in the surface. Adding all vertical relaxations yields for VASP-GGA a total surface compression of -0.13 Å for the 9-layer slab and -0.16 Å for the 15-layer calculation. These values are significantly smaller than those for the reconstructed surface which can be understood by the latter's greater openness and more degrees of freedom to relax.

C. Comparison and discussion of structural results

Table I summarizes our experimental and *ab initio* structural results for the Pt(110)-(1×2) MR structure (see Fig. 3) and compares them to those of earlier work. Evidently, there is an amazingly close correspondence between the structural parameter values determined in the present work experimentally by quantitative LEED and theoretically by DFT. Most of the values agree not only within the error limits estimated for the LEED analysis but deviate from each other by not more than 0.01 Å. The reader should note that though *average* interlayer spacings below the second layer are rather bulklike, atoms within these layers are well off their bulk positions due to buckling and pairing of atomic rows.

An exception of the almost perfect agreement between LEED and DFT seems to hold for the third layer buckling

which, though of the same order, differs by 0.06 Å between the two methods. Yet, even this deviation can in our opinion be traced back to a physical origin. While the DFT analysis describes a perfectly ordered (1×2) reconstructed surface of infinite extension, the real sample exhibits a vast number of steps as known through STM.[36,38] Below a step edge the buckled third layer has to match the unbuckled second and fourth layer of the neighboring terraces. Additionally, step relaxations as known from other stepped surfaces[69] will be superimposed and the overall structural matching may reduce the average buckling amplitude. In this light the agreement between LEED and DFT is rather good also with respect to the value of b_3. Interestingly, the LEED study of Ref. 37 deviates even more from the DFT result with respect to b_3, possibly due to a different step density. Generally, the different experimental LEED results listed in Table I agree rather well with each other except for those of Ref. 59, for which discrepancy we have no explanation. Reflection high-energy electron diffraction (RHEED) seems to overestimate the first layer contraction,[62,63] possibly due to nonconsideration of p_4. Small discrepancies with respect to results obtained by medium-energy ion scattering (MEIS) (Ref. 60) might also arise from neglecting some of the relaxations. The x-ray diffraction (XRD) results[61] are close to the LEED result given that XRD is more (less) accurate with respect to lateral (vertical) parameters than LEED.

We emphasize that the huge data base of our LEED analysis provides an unprecedented structural accuracy, possibly with exception of b_3 for which DFT should give the correct value in case of the ideal surface. In general, the agreement between DFT and LEED exhibits an impressive closeness of the structures independently retrieved, thus demonstrating today's achievable accuracy at a 10^{-2} Å level.

Quite surprisingly, only a few other theoretical results are available for the Pt(110)-(1×2) MR surface. The most recent work by Lee *et al.*[67] employs the *ab initio* FLAPW method in a very similar setup to our FLEUR calculations, i.e., LDA and a seven-layer (7L) thick single slab. Their results agree very well with present LEED data and also with our results for the much thicker 15L slab. However, in view of the discussion in the preceding section regarding the effects of slab thickness, especially their value for the buckling b_3 is quite remarkable. We like to emphasize at this point, that a 7L slab is too thin for the reliable calculation of b_3. In order to rule out any ambiguities regarding the accuracy of our methods, we recalculated a 7L Pt(110)-(1×2) MR slab with VASP using LDA and the same bulk lattice constant of 3.92 Å. Our results confirm the findings of Lee's FLAPW calculations, we obtain $b_3=0.27$ Å and $p_4=0.12$ Å. Thus we conclude that this apparently excellent agreement with experiment is due to the lack of the ''bulk'' in a 7L slab: the Pt atom in the third layer below the surface Pt rows does not have enough freedom to move into the ''bulk'' which is represented by only the center layer of the symmetric slab and leads to a smaller buckling (b_3) in this layer. Consequently, the pairing p_4 in the fourth layer is reduced since the repulsive force due to this third layer Pt atom is now smaller for the atoms in the central (fourth) layer. This trend is also noticeable in our other calculations: if b_3 is smaller (15L vs 9L), so is p_4. Comparing with other theoretical results one finds the largest deviations for the tight binding (TB) approach,[64] whereas the two calculations using the embedded atom method (EAM)—a bulk one[65] and its extension to surfaces[70]—yield reasonable results. Both the EAM and the TB approach are not *ab initio* methods, but rather depend on external parameters which makes them less suitable for the present purposes. Furthermore, these studies were mainly devoted to the structural stability of the Pt(110) surface, testing several models for the reconstruction by a comparison of total energies. Despite its shortcomings in predicting the geometry quantitatively, both methods find the MR reconstructed surface to be the stable one. We mention in this context that our 15L VASP calculations of course also favor the MR structure. It's energy is lower than that of the unreconstructed surface by 228 meV (GGA) [250 meV (LDA)]. This is actually the energy gain when the removed surface Pt chains are incorporated into the bulk.

The only other *ab initio* study among those listed in Table I, the local-orbital molecular dynamics (LOMD)[66] method, overestimates the compression of the first two interlayer spacings and, as a consequence, underestimates the buckling b_3. Although the LOMD method employs LDA, the calculated lattice parameter, which one would expect to be smaller than the experimental value, is closer to our GGA result which exceeds the experimental value by $\approx1.5\,\%$.

To our knowledge there are no experimental data available for the (1×1) structure of Pt(110), though it is known since long that it can be prepared as a metastable phase.[71,72] However, regarding the preparation recipe, which involves CO adsorption and subsequent electron stimulated desorption, the final cleanliness of such a surface remains at least questionable. Another possibility is epitaxial growth on, e.g., a Pd(110) substrate[73] which has a lattice constant only 0.8 % smaller than Pt and is known not to reconstruct. Unfortunately the unreconstructed (1×1) structure only exists up to a Pt coverage of two monolayers, then the usual (1×2) reconstruction sets in. The relaxations for the (1×1) structure determined by LEED, $\Delta d_{12}=-0.09$ Å and $\Delta d_{23}=0.06$ Å, are considerably smaller than our DFT results given in Table II, but nevertheless show the onset of an oscillatory relaxation profile. We also note that the relaxations obtained for the (1×2) reconstructed 3 ML Pt film are considerably smaller (e.g., $\Delta d_{12}=-0.15$ Å) than other results for the (110) surface of the Pt bulk. In view of the close correspondence between LEED and DFT results achieved for the clean reconstructed surface, DFT can be safely assumed to produce correct results for the (1×1) structure, too. This statement is reinforced by work on other (1×1) fcc(110) surfaces such as Ni(110),[74] Cu(110),[75] or Pd(110) (Ref. 76, and references therein), where good agreement between experiment and DFT calculations is found. According to these as well as to our present results the unreconstructed surface shows the typical oscillatory relaxation profile for open metal surfaces with a strong contraction of the first layer spacing and a smaller expansion for the second one. The third spacing is already almost bulklike due to effective electronic screening of the distortion introduced by the existence of the surface.

Concerning earlier theoretical results for Pt(110)-(1×1) (see Table II), to the best of our knowledge the only *ab initio* DFT calculation performed to yield an optimized geometry is within Feibelman's work on surface stress on fcc(110) surfaces.[77] The LDA calculation employs a LCAO method and a 13L slab, to model the surface. The published values are systematically smaller by about 30 %, but the oscillatory trend of the relaxation is nicely reproduced. In the last two rows theoretical data obtained by TB and EAM are listed. Not fully unexpected, the optimum geometries obtained disagree again with our present *ab initio* data. Despite its approximations, EAM still finds a Δd_{12} value very similar to ours. Yet it fails in predicting any reasonable further interlayer relaxation. Concerning the TB approach, we only agree on the sign of the relaxations. However, their amplitudes as determined by TB are smaller by at least a factor of 4.

Eventually, the reader should note that the average interlayer spacing d_{12} of the MR phase is very close to the same quantity of the unreconstructed surface. Some differences regarding d_{23} and d_{34} obviously arise from bucklings and pairings in the reconstructed surface. In the next section the DFT analysis of the clean Pt(110)-(1×1) surface will serve as a reference to understand the structural impact of bromine adsorption.

IV. COVALENT BONDING OF Br ON Pt(110): THE STRUCTURE OF THE $c(2\times2)$-Br/Pt(110) SURFACE

In a previous publication[16] part of the authors combined various experimental observations to deduce a substitutional adsorption site of bromine on Pt(110): First, only a minor change of the work function ($\Delta\phi_{\max}=100$ meV) and hence a small dipole moment was observed, in contrast to typical halogen adsorption induced changes in the eV region. Second, bromine atoms very dilutely adsorbed on the missing-row structure were identified as depressions in STM. So it appeared reasonable to transfer these results to the $c(2\times2)$ phase, where a pattern of alternating protrusions and depressions with practically the same corrugation is observed. Then, however, a bromine adsorption site considerably above the platinum surface plane cannot lead to a depression in STM without an enormous charge transfer which is incompatible with the small surface dipole moment observed. Third, substitutional adsorption would have allowed removal of the missing-row reconstruction by means of a purely local mass transport consistent with the observation of $c(2\times2)$ structural elements already at $T=420$ K. A further observation was the remarkable stability of Pt-Br-Pt chains on the $c(2\times2)$ surface. Consequently, a substitutional adsorption of Br had been postulated consisting of Pt-Br-Pt rows at the surface. All other experimental features could also be consistently interpreted in the framework of such an alternating chain model.

A. LEED analysis

For the reasons mentioned above, the LEED analysis concentrated at first on the substitution model. In order to save its local C_{2v} symmetry [see Fig. 4(a)] only vertical coordinates of atoms were varied. Using several Tensor LEED reference calculations the relative position of Br atoms with respect to the Pt atoms of the first layer was tested for both inward and outward relaxations. Additionally, the first Pt sublayer and the next four layers were allowed to shift vertically. However, none of these configurations achieved a Pendry R factor better than 0.73. Also, an imagined registry shift of the first layer by half a lattice parameter [Fig. 4(b)] did not improve the result ($R_P=0.80$). The same holds for a model with the bromine substitution assumed to take place in the third instead of the first layer [Fig. 4(c)] and so inducing a buckling in the top Pt layer which could alternatively account for the STM contrast observed. Yet, no combination of parameters produced an R factor below 0.77.

Therefore, the remaining class of adsorption models was examined, i.e., bromine atoms adsorbed *on* the surface [Figs. 4(d)–4(g)]. In a preliminary structural search, the high symmetry adsorption sites on-top, hollow, as well as long- and short-bridge were tested. While the first three models also led to R factors not lower than 0.77, the analysis of the short-bridge site instantaneously produced a Pendry R factor as low as 0.27. An additional fine-tuning of parameters, in particular lateral shifts and vibrations within this short-bridge model, further reduced the R factor to a final value of $R_P=0.23(1)$. Interestingly, the R factors for both subsets of integer and fractional order beam spectra are exactly the same. Also, practically the same quality of agreement is achieved as for the missing-row structure of the clean surface as visualized in Fig. 5. However, a peculiar feature of the LEED analysis should also be mentioned: The ratio of energy averaged intensities r between fractional and integer order beams is much higher in the calculations than in experiment ($r_{\mathrm{calc}}=0.44, r_{\mathrm{exp}}=0.12$). We attribute this to the instability of the $c(2\times2)$ structure against minor traces of contaminants originating from the filament of the electron gun (see Sec. IV C). With regard to our structural results, however, we emphasize at this point that it is rather unlikely to achieve a LEED fit quality as good as that above ($R_P=0.23$) with all other models failing at the level described ($R_P>0.73$). This makes us confident in the validity of the short-bridge model.

The structural parameters of the best-fit geometry are compiled in Table III. From the spacing d_{Br} between the bromine overlayer and the first platinum layer (together with the small lateral shift $p_{1,2}$ of the Pt atom) a Br-Pt bond length of $L=2.47$ Å results. This corresponds almost perfectly to the sum of the covalent radii of Pt and neutral Br, which amounts to $L^{\mathrm{atomic}}=2.495$ Å. The underlying substrate is still slightly relaxed with a 0.10 Å contraction of the first Pt interlayer spacing and a 0.03 Å expansion of the next one. Compared to the clean (1×1) structure of Pt(110) as derived from DFT (see Sec. III) this is equivalent to a roughly halfway derelaxation induced by the bromine adsorption. This is a typical feature known from many other adsorption systems.[68] The lateral shifts found in the analysis are minor and insignificant in view of the error limits involved. The vibrational amplitudes (not included in Table III) are largest for the Br atoms ($v_0=0.15\pm0.03$ Å) and still somewhat

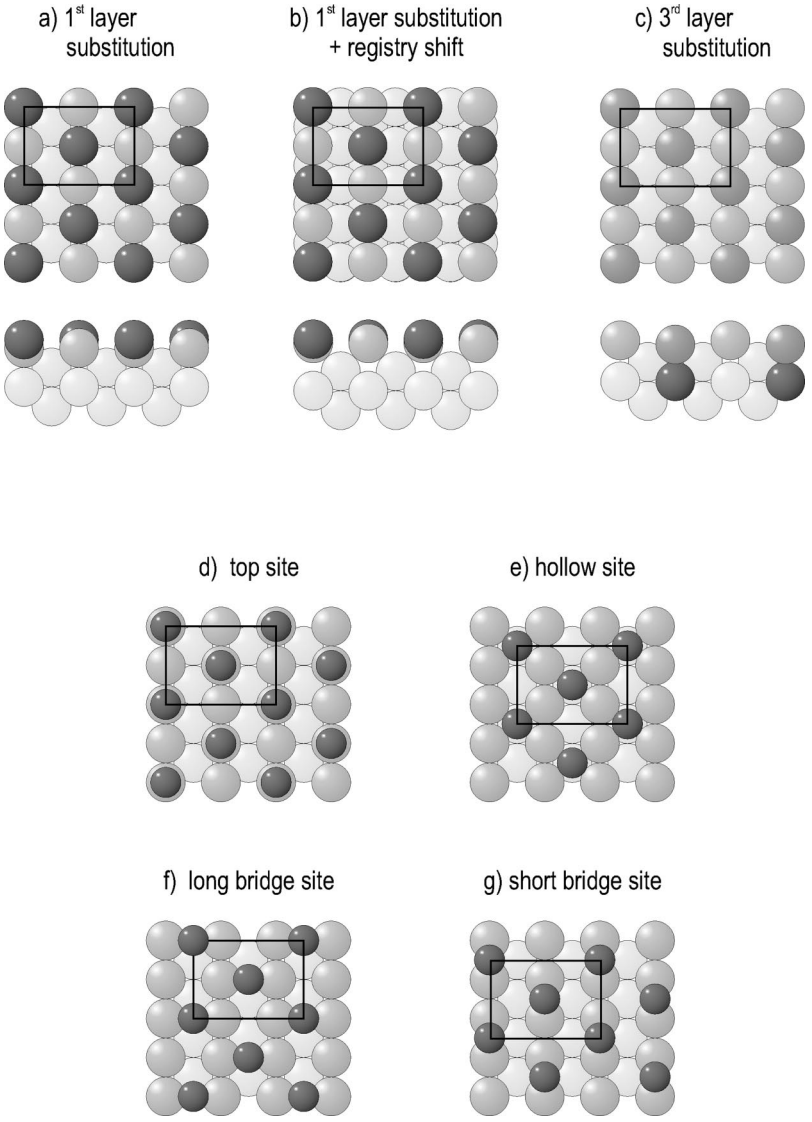

FIG. 4. Survey of the models tested in the LEED-I(E) analysis for the $c(2\times2)$-Br/Pt(110) structure.

increased in the uppermost two Pt layers ($v_1=0.11\pm0.04$ Å, $v_2=0.12\pm0.05$ Å) compared to the substrate bulk.

B. DFT analysis

In order to gain a deeper insight into the energetics of the adsorption model, we performed DFT calculations using the same setup as for the clean surface in Sec. III. The stability of a particular adsorption site is determined by the average adsorption energy per Br atom E_{ads}, defined as the difference in formation energies of a $c(2\times2)$ Br covered and a clean (1×1) Pt(110) 9L slab. The adsorption energies together with the corresponding Pendry R factors are listed in Table IV. The calculations show unambigously that adsorption on the short bridge site is favored, in perfect agreement with the LEED analysis.

The energetical ordering of the adsorption sites considered is independent of whether GGA or LDA is used, and even the least favorable direct hollow Br adsorption site is more stable by ~0.7 eV than a substitutional model. The absolute value of $E_{\mathrm{ads}}^{\mathrm{LDA}}$ is always larger than that of $E_{\mathrm{ads}}^{\mathrm{GGA}}$ reflecting the well known tendency of LDA to overbind. Another tendency of LDA clearly visible is its favoring of highly coordinated sites. $E_{\mathrm{ads}}^{\mathrm{LDA}}$ is larger than $E_{\mathrm{ads}}^{\mathrm{GGA}}$ for the top site by 0.58 eV, by 0.69(71) eV for the short (long) bridge and by 0.77 eV for the hollow site.

The optimum relaxed geometry for the favorable Br adsorption on the short bridge site using different theoretical setups is given in Table III. It is interesting to note that most of the relaxations take place near the surface, in contrast to the clean (reconstructed) surface where relaxations involve atoms down to the fourth layer. Therefore the thickness of the slab (9L vs 15L) is of only minor importance. Similar to the clean surfaces, differences between VASP and FLEUR results are well within the experimental error limits. Actually, the largest differences are found for the distance between Br and the Pt(110) substrate using either LDA or GGA potentials. Compared to GGA, the tendency of LDA to overbind leads to smaller values of d_{Br} by 0.05–0.07 Å, the difference being only slightly larger than the experimental error margin of ±0.03 Å. It should be noted that the present

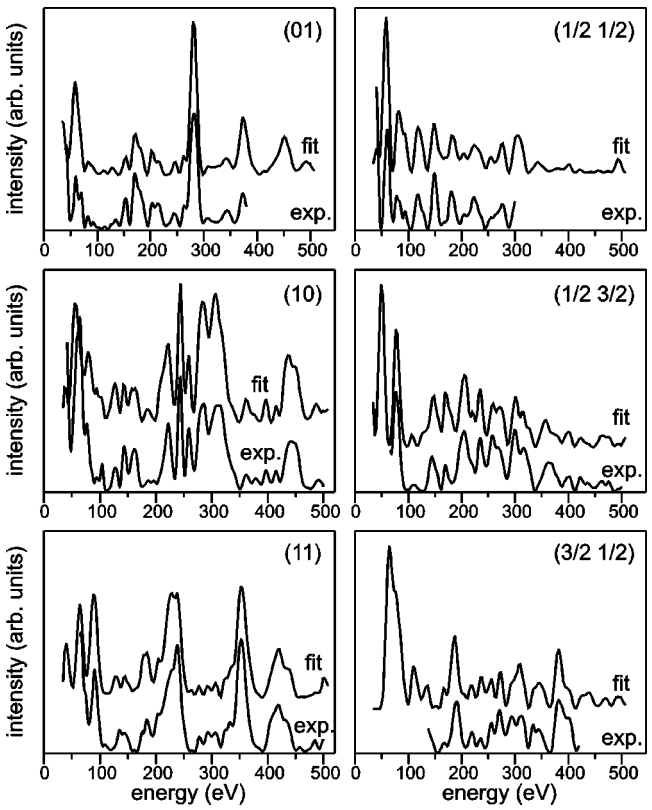

FIG. 5. Comparison of experimental and calculated best-fit LEED-$I(E)$ spectra for $c(2\times2)$-Br/Pt(110).

$c(2\times2)$-Br/Pt(110) overlayer and a $p(2\times1)$-Br/Pt(110) overlayer with Br in the short-bridge sites are energetically degenerate within the error limits of the present calculation; this is consistent with our previous experimental result.[16]

C. Discussion

In the following we first address the reliability of the present structure determination and compare the results obtained experimentally by quantitative LEED and through first-principle calculations applying DFT. Then we show that the main experimental results of Ref. 16, namely, the small value of the work function change along with the observed negative constrast of Br in STM for low coverages as well as the nonlocal mass transport and the stability of Br-bridged Pt chains—which had been interpreted by a substitutional model—can easily be reconciled with the new short-bridge model.

TABLE IV. Atomic bromine adsorption energies E_{ads} for different Br/Pt(110) adsorption models calculated with VASP using both GGA and LDA potentials. The corresponding best-fit Pendry R factors R_P of the LEED analysis are also included for comparison. The first four models refer to direct adsorption of Br *on* the Pt(110) surface. The last line refers to the substitutional model [Fig. 3(a)] originally suggested in Ref. 16.

model	$E_{\mathrm{ads}}^{\mathrm{GGA}}$(eV)	$E_{\mathrm{ads}}^{\mathrm{LDA}}$(eV)	R_P
$c(2\times2)$ short bridge	−3.28	−3.97	0.23
$c(2\times2)$ long bridge	−3.13	3.84	0.77
$c(2\times2)$ top	−2.92	−3.50	0.78
$c(2\times2)$ hollow	−2.56	−3.33	0.77
$c(2\times2)$ substitution	−1.80	−2.62	0.73

(i) *Reliability of the structure determination.* The results of the experimental and theoretical structure determination of the $c(2\times2)$-Br/Pt(110) surface not only exhibit excellent quantitative agreement as apparent from Table III. They both appear to be on very safe grounds on their own.

Concerning LEED, only the adsorption model involving the short bridge site produced a convincing fit between experiment and model calculations ($R_P=0.23$). The R factors of *all* other models (substitutional or other adsorption sites) were not only much above the R-factor variance level but with $R_P>0.73$ approaching the range where calculated and experimental intensity spectra become uncorrelated. This behavior is due to the extreme and unusual structural richness of the spectra as visualized in Fig. 5 (a feature applying also to the data of the clean surface). Only the correct model can reproduce the many peaks over the large energy range considered ($\Delta E=4586$ eV), a width which is not routine even in today's structure analyses. The reader should also note that not only the peak positions (on which the Pendry R factor focuses) are reproduced but to a high degree also the relative intensities within each spectrum.

TABLE III. LEED and DFT results for the Br/Pt(110)−$c(2\times2)$ phase. d_{Br} denotes the Br-substrate distance, $\Delta d_{i,i+1}$ the changes in the interlayer spacing with respect to the ideal bulk spacing d_0, and p_i the lateral pairing in layer i, all values given in Å. Signs of the lateral pairing parameters p_i are given with respect to the position of the Br atoms. Error limits for the parameters derived by LEED (neglecting parameter correlations) are ±0.03 Å for d_{Br} and $\Delta d_{i,i+1}$, ±0.08 Å for p_1 and ±0.10 Å for p_2. (L: number of layers considered in the calculations.)

Method	d_{Br}	Δd_{12}	Δd_{23}	Δd_{34}	Δd_{45}	p_1	p_2	p_3	p_4	d_0
LEED	2.04	−0.10	0.03	0.01	0.00	0.04	−0.04			1.385
VASP-LDA-15L	2.02	−0.12	0.03	0.01	0.01	0.01	−0.01	0.02	−0.01	1.382
VASP-GGA-15L	2.09	−0.11	0.03	0.02	0.01	0.01	−0.04	0.02	−0.03	1.408
VASP-LDA-9L	2.04	−0.11	0.02	0.03		0.00	−0.02	0.01	0.00	1.382
VASP-GGA-9L	2.09	−0.11	0.02	0.02		0.01	−0.04	0.01	−0.02	1.408
FLEUR-GGA-9L	2.11	−0.12	0.01	−0.01		0.05	−0.06	0.01	0.00	1.405

TABLE V. Metal-halogen bondlength, metal-halogen layer distance z and work function change $\Delta\Phi$.

System	Adsorption site	Bond length	z	$\Delta\Phi$ (meV)	Refs.
Br/Pt(110)$-c(2\times2)$	short bridge	2.47 Å	2.05 Å	100	this work
Cl/Pt(110)$-p(2\times1)$	short bridge	2.38 Å	1.93 Å	550	6,87
Cl/Ag(100)$-c(2\times2)$	fourfold hollow	2.61$-$2.69 Å	1.62$-$1.75 Å	1700	24,31,88
Cl/Ag(111)$-\sqrt{3}\times\sqrt{3}R30°$	fcc site	2.48$-$2.70 Å	1.83$-$2.12 Å	1400	20,89–91
Cl/Ag(110)$-p(2\times1)$	fourfold hollow[a]	2.56 Å	0.53 Å	1050	21,92
Cl/Cu(100)$-c(2\times2)$	fourfold hollow	2.37$-$2.41 Å	1.54$-$1.60 Å	1100	18,25,26
Cl/Cu(111)$-\sqrt{3}\times\sqrt{3}R30°$	fcc site	2.39 Å	1.88 Å	900	30,27,93
I/Ag(110)	short bridge	3.11 Å	2.75 Å	1000	92,28
I/Cu(100)$-p(2\times2)$	fourfold hollow	2.69 Å	1.99 Å		94,95
Br/Ag(110)$-p(2\times1)$				1000	8
Br/Cu(100)$-c(2\times2)$				900	96
Cl/Ni(110)$-c(2\times2)$				1100	6
Cl/Pd(110)$-c(2\times2)$				1200	6
Cl/Ni(111)$-\sqrt{3}\times\sqrt{3}R30°$				380	97
Cl/Pd(111)$-\sqrt{3}\times\sqrt{3}R30°$				260	96
Cl/Pt(111)-3×3				100	85
Br/Pd(111)$-\sqrt{3}\times\sqrt{3}R30°$				350	98
Br/Pt(111)-3×3				80	10

[a]Assumed.

As mentioned in Sec. IV A the ratio of energy averaged intensities r between fractional and integer order beams is much higher in the calculations than in experiment ($r_{\mathrm{calc}}=0.44$, $r_{\mathrm{exp}}=0.12$). The simplest explanation would be that part of the surface exhibits (1×1) rather than $c(2\times2)$ order, consistent with the fact that relative intensities of spectra within the subsets of beams are well reproduced. Yet, electron-induced desorption can be ruled out from test experiments and the occurrence of (1×1) domains is in contrast to the STM observations. Alternatively and also consistent with relative intensities measured for beam subsets, the low r value can be interpreted as being due to substantial intrinsic disorder. Again, this seems to be at variance with STM investigations [see Ref. 16 and Fig. 1(a)] which find large and well ordered $c(2\times2)$ domains in agreement with the observation that the half-width of all LEED spots is determined by the transfer width of the optics. On the other hand, it is also observed that adsorption of small amounts of halogens, NO and CO quickly destroys the $c(2\times2)$ structure [eventually leading to a (3×1) superstructure[78–80]]. Yet, this does not destroy the coherence between the remaining ordered adatoms, so the half-width of fractional order spots remains constant though their intensity decreases. This decrease should be more rapid than that of integer order spots because the ordered bulk below the disordered parts of the overlayer also contributes to the integral spots. The disturbing CO molecules seem to originate from the filament of the electron gun as checked by time dependent measurements of the intensity of an integral and a fractional spot at a fixed electron energy displayed in Fig. 1(d). Evidently, the intensity of the fractional order spot decreases much more rapidly. This result suggests that the low intensity of the experimental fractional order spots may be attributed to disorder induced by traces of CO originating from the filament of the LEED gun whereby, however, there are still large and well ordered $c(2\times2)$ domains accounting for sharp superstructure spots.

The DFT results are equally convincing on their own. There are only little differences between parameters obtained by all-electron full potential augmented plane wave (FLEUR) and projector augmented wave (VASP) methods and by comparing the 9L and 15L results the calculations appear well converged with respect to the slab thickness. Similarly, using a free standing single slab model (FLEUR) or a repeated slab model (VASP) makes no difference. Last but not least the comparison to the LEED result is excellent, which proves that the *ab initio* DFT packages FLEUR and VASP represent one of the most accurate approaches available today. The almost quantitative agreement between LEED and DFT applies in particular to all relaxational parameters of the substrate Pt(110) which agree well within the error limits. Even the change of sign and also the magnitude of the small lateral pairings p_1 and p_2 are nicely reproduced. There is only a small deviation (~0.05 Å) concerning the GGA calculations of d_{Br} which is slightly outside the experimental error limits. However, this overestimated Pt-Br bond-length is still within the expected GGA error limits and is certainly altered by an improved GGA functional.

(ii) *Low work function change*. The measured change $\Delta\Phi$ of the work function caused by the transition from the Pt(110)-(1×2)MR to the $c(2\times2)$-Br/Pt(110) surface is $\Delta\Phi\approx70$ meV.[16] The present DFT calculations yield an almost negligible work function change too. This is in marked contrast to halogen-Cu or halogen-Ag adsorption systems (see Table V) with work function changes of the order of 1–2 eV.[81] While, in the absence of direct structural information, substitutional adsorption seemed to provide the most natural explanation,[16] the DFT calculation and LEED results demand an alternative interpretation. Clearly, the alternative in

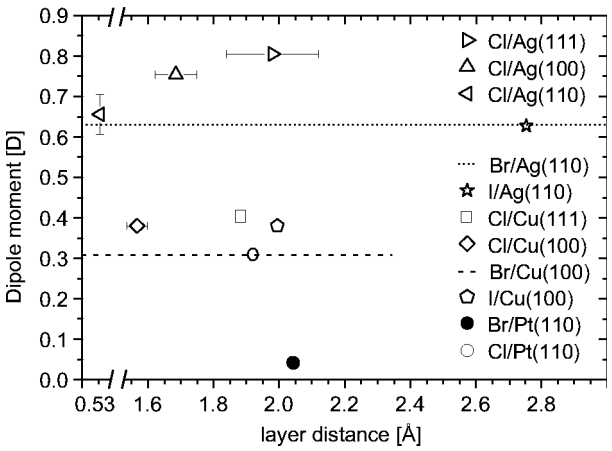

FIG. 6. Dipole moment per halogen atom versus halogen-metal layer distance. The symbols represent different experimental and theoretical results for the adsorption of Cl, Br, and I on Ag, Cu, and Pt surfaces (see Table V). Error bars indicate the scatter in the reported values for the bond length. Typical errors in the work function change measurements result in an uncertainty of the dipole moment of $\pm 0.05D$. Br/Pt(110): this work, Cl/Pt(110)(Refs. 6,87), Cl/Ag(111) (Refs. 20,89–91), Cl/Ag(100) (Refs. 24,31,88), Cl/Ag(110) (Refs. 21,92), Br/Ag(110) (Ref. 8) (no structural data), I/Ag(110) (Refs. 92,28), Cl/Cu(111) (Refs. 30,27,93), Cl/Cu(100) (Refs. 18,25,26), Br/Cu(100) (Ref. 96) (no structural data); I/Cu(100) (Refs. 94,95).

this case is to attribute the low work function change to covalent instead of ionic bonding usually assumed for halogen-metal bonding. The covalent bond character seems to be specific for Pt (and—to a lesser extent—the other d^9 transition metals) as indicated in Table V; both Cl and Br cause anomalously low work function changes on Pt(111) as well. Figure 6 shows a plot of the dipole moment per halogen atom versus the distance between the halogen layer and the first metal layer, for different halogen-metal systems. The resulting dipole moments depend on the substrate and appear to be grouped around a distinct value for each metal: The dipole moment is larger for Ag ($p=0.7D$) than for Cu ($p=0.35D$), whereas for Br/Pt(110) we find an anomalously small value of $p=0.04D$. For Ag and for Cu the variation of the dipole moment with surface orientation and halogen species, and hence the halogen-metal layer distance, is small. The comparatively large difference between the dipole moment of Cl/Pt(110) and Br/Pt(110) seems to be not in line, but the Cl data are taken from an early measurement, where Cl was dosed by exposure to ambient Cl_2 atmosphere.[6] Qualitatively the difference in dipole moments is in line with the electronegativity difference between Cl and Br. Note that the dipole moments given here refer to coverages in the monolayer range. Depolarization effects are not taken into account. In summary, for Br/Pt(110) we can exclude an ionic bonding model. This corroborates our previous arguments for covalent bonding and a covalent poisoning mechanism[82] which were based on photoemission results.

(iii) *Local versus nonlocal mass transport*. In Ref. 16 the substitutional adsorption model was favored, because it required only local platinum transport to form a $c(2\times2)$ structure. Within the present short-bridge adsorption model, the mass transport lifting the missing-row reconstruction is different, but still rather local and analogous to the CO induced lifting of the Pt(110)-(1×2) missing-row reconstruction.[83] It is entirely consistent with the experimental data of Ref. 16. At room temperature, Br forms a (2×2) overlayer on the (1×2) missing-row reconstructed Pt(110) surface.[16] Formation of vacancy islands within the topmost Pt layer starts after annealing to 370 K. The displaced Pt atoms reside in the troughs of the remaining missing-row areas and form crosslike structures or a square grid pattern.[16] At successively higher annealing temperatures the vacancy islands grow and the Pt atom density in the remaining first layer troughs increases until locally a (1×1) structure prevails. At this stage (annealing to 420 K) the surface consists of irregularly shaped (1×1) domains of partly the first and partly the second Pt layer. On a mesoscopic scale the pattern is strongly reminiscent to the one formed by CO on Pt(110).[83] The adsorbed Br forms mixed $p(2\times1)$ and $c(2\times2)$ overlayer structures on both, the first and the second layer (1×1) domains. At $\Theta=0.5$ ML Br desorbs only at $T=800$ K. Consequently, the surface can be annealed at 780 K without loss of Br. At this temperature the mobility is high enough to allow formation of large, almost perfectly developed $c(2\times2)$-Br/Pt(110) terraces [see Fig. 1(a)].

(iv) *Stability of the Br-bridged Pt chains*. By heating to 800 K the $c(2\times2)$ structure is object to a slight loss of Br. As a result, a missing-added-row reconstruction starts to develop. The single added rows exhibit the typical Br induced corrugation.[16] In Refs. 16 and 5 the stability of these rows was interpreted as a tendency to form linear Pt-Br-Pt chains in analogy to the quasi-one-dimensional halogen-bridged Pt linear chain compounds.[4] In the light of the present structural model the added rows have to be interpreted as close-packed Pt rows bearing an adsorbed Br atom on every second short-bridge site. The implications are twofold. First, even a slight substoichiometry of the $c(2\times2)$ structure triggers an instability towards a missing-row reconstruction. Note that for every Br atom lost, on average seven Pt atoms are expelled from the surface layer. Second, the added rows are always fully occupied by Br atoms in every second bridge site indicating a peculiar stability of these Br-bridged Pt chains not only in the $c(2\times2)$ or $p(2\times1)$ structure, but also as solitary chains on flat terraces. Both observations clearly point to a substantial anisotropy, that is to say a quasi-one-dimensionality, of the Br-bridged Pt chains as already concluded in Refs. 16 and 5.

(v) *STM contrast*. Figure 1(a) shows an STM image of the $c(2\times2)$-Br/Pt(110) structure. From this image neither the adsorption site nor the chemical contrast of Br can be deduced. DFT calculations indicate that Br is imaged as protrusion [see Fig. 1(b)]. Constant current STM images have been calculated on the basis of the Tersoff-Hamann model,[84] which yields a tunneling current $I(z)$ proportional to the sample's local density of states (LDOS) $\rho_S(z,E)$ at the position z of the tip above the surface. Only states of energy E satisfying resonant tunneling conditions for the applied bias voltage are considered. Simulating the present experimental STM image the LDOS $\rho_S(z,E)$ was integrated between E

$=E_F$ and $E=E_F+820$ meV. The isosurface of constant LDOS (current) displayed in Fig. 1(b) shows a corrugation of 0.25 Å close to the experimental findings. The tip-sample distance leading to this corrugation is calculated to be around 6 Å with respect to the top Pt layer ($\sim$4 Å with respect to the Br), quite typical for metallic surfaces. Hence, in the STM images of the $c(2\times2)$ structure the bright spots have to be interpreted as Br atoms and the dark spots as empty short-bridge sites. For small Br coverages STM images showed depressions in the close-packed rows on the missing-row reconstructed surface. They were interpreted as Br dimers.[16] New results, of both, STM experiments and DFT calculations, however, question this interpretation. Hence additional experiments are presently underway in order to clarify the adsorption structure at low coverage.

V. SUMMARY

We have carried out a structure analysis of the $c(2\times2)$-Br/Pt(110) surface by quantitative LEED analysis and by first principles DFT calculations. The latter were carried out by using a full-potential linearized augmented plane wave method as implemented in the FLEUR code,[51] as well as a pseudopotential projector augmented wave method (VASP code).[52] In addition, the missing-row reconstructed clean Pt(110) surface was reanalyzed and compared to previously reported results. The LEED analysis was carried out with an extraordinary broad database and shows a remarkable convergence with the results of the first-principles calculations. This proofs that state-of-the-art calculational methods have matured to a complete tool-box for structure determination rivaling present-day experimental methods with respect to precision and reliability. Encouraged by this result, we also calculated the geometry of the unreconstructed (1×1) Pt(110) surface in order to assess changes in the geometry for adsorption systems where the reconstruction is lifted.

As expected, only the precision of earlier structure determinations was improved for the clean (1×2) MR reconstructed Pt(110) surface. For the $c(2\times2)$-Br/Pt(110) system, however, the previous structural assignment[16] had to be revised: Instead of substitutional adsorption with essentially colinear Pt-Br-Pt chains the present study finds simple adsorption with every second short-bridge site on the Pt chains being occupied by Br. The missing-row reconstruction is lifted. As usual, the first interlayer contraction in the substrate is seen to be significantly reduced in the adsorption system. Remarkably, the Br-Pt bonding distance amounts almost precisely to the sum of the covalent radii indicating essentially covalent bonding. A covalent bonding is also indicated by the experimental work function and photoemission data.[16,82]

Finally, theoretical STM images were calculated on the basis of the Tersoff-Hamann formalism. They unequivocally show Br imaged as protrusion in contrast to the previously given interpretation of the STM images.[16] The present study provides therefore a further example for the difficulty to obtain reliable structure assignments solely on the basis of STM and qualitative LEED measurements.

ACKNOWLEDGMENT

This work was supported by the Austrian Science Fund.

*Also at: Istituto Nazionale di Fisica della Materia (INFM), Dipartimento di Scienze Fisiche, Università degli Studi di Cagliari I–09124 Cagliari, Italy.

[1] H.F. Winter and J.W. Coburn, Surf. Sci. Rep. **14**, 161 (1992).
[2] R.G. Jones, Prog. Surf. Sci. **27**, 25 (1988).
[3] T.W. Fishlock, J.B. Pethica, and R.G. Egdell, Surf. Sci. **445**, L47 (2000).
[4] M. Alouani, J.M. Wilkins, R.C. Albers, and J.M. Wills, Phys. Rev. Lett. **71**, 1415 (1993).
[5] K. Swamy, A. Menzel, R. Beer, and E. Bertel, Phys. Rev. Lett. **86**, 1299 (2001).
[6] W. Erley, Surf. Sci. **114**, 47 (1982).
[7] B. Krüger and C. Benndorf, Surf. Sci. **177**, 515 (1986).
[8] C. Benndorf and B. Krüger, Surf. Sci. **151**, 271 (1985).
[9] H.-G. Zimmer, A. Goldmann, R. Courths, and H. Saalfeld, Surf. Sci. **173**, 465 (1986).
[10] E. Bertel, K. Schwaha, and F. Netzer, Surf. Sci. **83**, 439 (1979).
[11] E. Bertel and F. Netzer, Surf. Sci. **97**, 409 (1980).
[12] T.W. Fishlock, J.B. Pethica, F.H. Jones, R.G. Egdell, and J.S. Foord, Surf. Sci. **312**, 629 (1997).
[13] H. Xu, R. Yuro, and I. Harrison, Surf. Sci. **411**, 303 (1998).
[14] C.Y. Nakakura and E.I. Altman, Surf. Sci. **398**, 281 (1998).
[15] T.W. Fishlock, J.B. Pethica, A. Oral, R.G. Egdell, and F.H. Jones, Surf. Sci. **426**, 212 (1999).
[16] K. Swamy, P. Hanesch, P. Sandl, and E. Bertel, Surf. Sci. **466**, 11 (2000).
[17] P. Citrin, P. Eisenberger, and R.C. Hewitt, Phys. Rev. Lett. **45**, 1948 (1981).
[18] P.H. Citrin, D.R. Hamann, L.F. Mattheiss, and J.E. Rowe, Phys. Rev. Lett. **49**, 1712 (1982).
[19] M. Crapper, C. Riley, P. Sweeney, C. McConville, D. Woodruff, and R. Jones, Europhys. Lett. **2**, 857 (1986).
[20] G. Lamble, R. Brooks, S. Ferrer, D.A. King, and D. Norman, Phys. Rev. B **34**, 2975 (1986).
[21] D.J. Holmes, N. Panagiotides, R. Dus, D. Norman, G.M. Lamble, C.J. Barnes, F. Della Valla, and D.A. King, J. Vac. Sci. Technol. A **5**, 703 (1987).
[22] G. Lamble, R.S. Brooks, J.-C. Campuzana, D.A. King, and D. Norman, Phys. Rev. B **36**, 1796 (1987).
[23] M. Kiguchi, T. Yokoyama, S. Terada, M. Sakano, Y. Okamoto, T. Ohta, Y. Kitajima, and H. Kuroda, Phys. Rev. B **56**, 1561 (1997).
[24] E. Zanazzi, F. Jona, D.W. Jepsen, and P.M. Marcus, Phys. Rev. B **14**, 432 (1976).
[25] D. Westphal, A. Goldmann, F. Jona, and P.M. Marcus, Solid State Commun. **44**, 1712 (1982).
[26] F. Jona, D. Westphal, A. Goldmann, and P. Marcus, J. Phys. C **16**, 3001 (1983).
[27] K. Doll and N.M. Harrison, Chem. Phys. Lett. **317**, 282 (2000).
[28] H.-R. Tang, W.-N. Wang, Z.-H. Li, W.-L. Dai, K.-N. Fan, and J.-F. Deng, Surf. Sci. **450**, 133 (2000).
[29] K. Kleinherbers and A. Goldmann, Fresenius' Z. Anal. Chem. **329**, 285 (1987).

[30] D. Woodruff, D.L. Seymour, C.F. McConville, C.E. Riley, M.D. Crapper, N.P. Prince, and R.G. Jones, Phys. Rev. Lett. **58**, 1460 (1987).
[31] F. Jona and P. Marcus, Phys. Rev. Lett. **50**, 1823 (1983).
[32] K. Swamy, E. Laegsgard, and F. Besenbacher (unpublished).
[33] Rasterscope 3000, DME, Herlev, Denmark.
[34] SPM 100, RHK Technology, Michigan, USA.
[35] ErLEED 3000, Specs, Berlin, Germany.
[36] P. Hanesch and E. Bertel, Phys. Rev. Lett. **79**, 1523 (1997).
[37] P. Fery, W. Moritz, and D. Wolf, Phys. Rev. B **38**, 7275 (1988).
[38] K. Swamy, E. Bertel, and I. Vilfan, Surf. Sci. **425**, L369 (1999).
[39] SensiCam, PCO Computer Optics, Kelheim, Germany.
[40] V. Blum and K. Heinz, Comput. Phys. Commun. **134**, 392 (2001).
[41] P. Rous, J. Pendry, D. Saldin, K. Heinz, K. Müller, and N. Bickel, Phys. Rev. Lett. **57**, 2951 (1986).
[42] P. Rous and J. Pendry, Surf. Sci. **219**, 355 (1989); **219**, 373 (1989).
[43] P. Rous, Prog. Surf. Sci. **39**, 3 (1992).
[44] K. Heinz, Rep. Prog. Phys. **58**, 637 (1995).
[45] K. Heinz, M. Kottcke, U. Löffler, and R. Döll, Surf. Sci. **357-358**, 1 (1996).
[46] M. Kottcke and K. Heinz, Surf. Sci. **376**, 352 (1996).
[47] J. Pendry, J. Phys. C **13**, 937 (1980).
[48] J. Rundgren, Phys. Rev. B **59**, 5106 (1999).
[49] S. Müller, Ph. D. thesis, University Erlangen-Nürnberg, 1996.
[50] M. Weinert, E. Wimmer, and A. Freeman, Phys. Rev. B **26**, 4571 (1982).
[51] URL: http://www. flapw.de.
[52] G. Kresse and J. Furthmüller, Comput. Mater. Sci. **54**, 11 169 (1996).
[53] P.E. Blöchl, Phys. Rev. B **50**, 17 953 (1994).
[54] G. Kresse and D. Joubert, Phys. Rev. B **59**, 1758 (1999).
[55] Y. Wang and J.P. Perdew, Phys. Rev. B **44**, 13 298 (1991).
[56] J.P. Perdew and A. Zunger, Phys. Rev. B **23**, 5048 (1981).
[57] D.M. Ceperley and B.J. Alder, Phys. Rev. Lett. **45**, 566 (1980).
[58] S.L. Cunningham, Phys. Rev. B **10**, 4988 (1974).
[59] E.C. Sowa, M.A. van Hove, and D.L. Adams, Surf. Sci. **199**, 174 (1988).
[60] P. Fenter and T. Gustafsson, Phys. Rev. B **38**, 10 197 (1988).
[61] E. Vlieg, I. Robinson, and K. Kern, Surf. Sci. **233**, 248 (1990).
[62] M. Stock, J.R.U. Korte, and G. Meyer-Emsen, Surf. Sci. **233**, L243 (1990).
[63] U. Korte and G. Meyer-Ehmsen, Surf. Sci. **271**, 616 (1992).
[64] H.-J. Brocksch and K. Bennemann, Surf. Sci. **161**, 321 (1985).
[65] S. Foiles, Surf. Sci. **191**, L779 (1987).
[66] M.-H. Tsai and K. Hass, Phys. Rev. B **52**, 16 420 (1995).
[67] J.I. Lee, W. Mannstadt, and A.J. Freeman, Phys. Rev. B **59**, 1673 (1999).
[68] P. Watson, M. V. Hove, and K. Hermann, NIST Surface Structure Database - Ver. 3.0, National Institute of Standards and Technology, Gaithersburg, MD, 1999.
[69] S. Walter, H. Baier, M. Weinelt, K. Heinz, and T. Fauster, Phys. Rev. B **63**, 155407 (2001).
[70] M. Haftel, Phys. Rev. B **48**, 2611 (1993).
[71] C. Comrie and R. Lambert, J. Chem. Soc., Faraday Trans. **72**, 1659 (1976).
[72] S. Ferrer and H. Bonzel, Surf. Sci. **119**, 234 (1982).
[73] O.L. Warren, H. Kang, P.J. Schmitz, P.A. Thiel, P. Kaukasoina, and M. Lindroos, Phys. Rev. B **47**, 10 839 (1993).
[74] F. Mittendorfer, A. Eichler, and J. Hafner, Surf. Sci. **423**, 1 (1999).
[75] J. Redinger, P. Weinberger, H. Erschbaumer, R. Podloucky, C.L. Fu, and A.J. Freeman, Phys. Rev. B **44**, 8288 (1991).
[76] V. Ledentu, W. Dong, P. Sautet, G. Kresse, and J. Hafner, Phys. Rev. B **57**, 12 482 (1998).
[77] P.J. Feibelman, Phys. Rev. B **51**, 17 867 (1995).
[78] C. Deisl, K. Swamy, S. Penner, and E. Bertel, Phys. Chem. Chem. Phys. **3**, 1213 (2001).
[79] K. Swamy, A. Menzel, R. Beer, C. Deisl, S. Penner, and E. Bertel, Surf. Sci. **482-485**, 402 (2001).
[80] K. Swamy, C. Deisl, A. Menzel, R. Beer, S. Penner, and E. Bertel (unpublished).
[81] For Cl and Br on Pt(111) a sign reversal of the work function change is observed at low coverages. Substitutional adsorption was proposed as a possible explanation (Refs. 10,85).
[82] A. Menzel, K. Swamy, R. Beer, P. Hanesch, E. Bertel, and U. Birkenheuer, Surf. Sci. **454-456**, 88 (2000).
[83] T. Gritsch, D. Coulman, R.J. Behm, and G. Ertl, Phys. Rev. Lett. **63**, 1086 (1989).
[84] J. Tersoff and D.R. Hamann, Phys. Rev. B **31**, 805 (1985).
[85] W. Erley, Surf. Sci. **84**, 281 (1980).
[86] S. Foiles, M. Baskes, and M. Daw, Phys. Rev. B **33**, 7983 (1986).
[87] C. Deisl, K. Swamy, E. Bertel, C. Franchini, J. Redinger, S. Walther, L. Hammer, and K. Heinz (unpublished).
[88] K. Kleinherbers, E. Janssen, A. Goldmann, and H. Saalfeld, Surf. Sci. **215**, 394 (1989).
[89] A. Shard and V.R. Dhanak, J. Phys. Chem. B **104**, 2732 (2000).
[90] K. Doll and N.M. Harrison, Phys. Rev. B **63**, 165410 (2001).
[91] K. Kleinherbers, Ph. D. thesis, Duisburg, 1987.
[92] H. Hinzert, K.K. Kleinherbers, E. Janssen, and A. Goldmann, Appl. Phys. A: Mater. Sci. Process. **49**, 313 (1989).
[93] K. Kleinherbers and A. Goldmann, Surf. Sci. **154**, 489 (1985).
[94] P. Citrin, P. Eisenberger, and R.C. Hewitt, Phys. Rev. Lett. **45**, 1948 (1980).
[95] S.B. DiCenzo, K. Wertheim, and D. Buchanan, Phys. Rev. B **24**, 6143 (1981).
[96] K. Kleinherbers, H.-G. Zimmer, and A. Goldmann, Surf. Sci. **167**, 417 (1986).
[97] W. Erley and H. Wagner, Surf. Sci. **66**, 371 (1977).
[98] W.T. Tysoe and R.M. Lambert, Surf. Sci. **115**, 37 (1982).